Applied Thermal Engineering 182 (2021) 116099

Contents lists available at ScienceDirect

Applied Thermal Engineering

journal homepage: www.elsevier.com/locate/apthermeng

Unsteady ultra-lean combustion of methane and biogas in a porous burner – An experimental study

Rabeeah Habib [a], Bijan Yadollahi [a], Ali Saeed [a], Mohammad Hossein Doranehgard [b], Larry K. B. Li [c], Nader Karimi [a,d,*]

[a] James Watt School of Engineering, University of Glasgow, Glasgow G12 8QQ, United Kingdom
[b] Department of Civil and Environmental Engineering, School of Mining and Petroleum Engineering, University of Alberta, Edmonton, Alberta T6G 1H9, Canada
[c] Department of Mechanical and Aerospace Engineering, Hong Kong University of Science and Technology, Clear Water Bay, Hong Kong
[d] School of Engineering and Materials Science, Queen Mary University of London, London E1 4NS, United Kingdom

ARTICLE INFO

Keywords:
Ultra-lean combustion
Biogas combustion
Porous burner
Unsteady combustion
Forced response

ABSTRACT

The response of ultra-lean flames, stabilised in a porous burner, to the fluctuations imposed on the fuel flow rate is investigated experimentally. The study is motivated by the likelihood of small biogas generators to produce fuels with temporal variations in their flow rate and chemical composition. The employed porous burner includes layers of silicon carbide porous foam placed inside a quartz tube. The burner is equipped with a series of axially arranged thermocouples and is imaged by a digital camera. Methane and a blend of methane and carbon dioxide (mimicking biogas) are mixed with air and then fed to the burner at equivalence ratios below 0.3. The fuel flow rate is modulated with a programmable mass flow controller by imposing a sinusoidal wave with variable amplitude and frequency on the steady fuel flow. Through analysis of the flame images and collected temperature traces, it is shown that the imposed disturbances result in motion of the flame inside the burner. Such motion is found to qualitatively follow the temporal variation in the fuel flow for both methane and biogas. Nonetheless, the amplitude of the flame oscillations for methane is found to be higher than that for biogas. Further, it is observed that exposure of the burner to the fuel fluctuations for a long time (180 s) eventually results in flame destabilisation. However, stabilised combustion was achieved for methane mixtures at amplitudes between 0 and 30% of steady values over a period of 60 s. This study reveals the strong effects of unsteady heat transfer in porous media upon the fluctuations in flame position.

1. Introduction

Utilisation of low-calorific fuels can improve energy efficiency and reduce carbon emissions by combustion systems [1]. In particular, combustion of carbon neutral, low-calorific fuels is of high significance in lowering CO_2 emissions [2–4]. Yet, combustion of low-calorific fuels often involves significant challenges regarding flame stability in most conventional burners [5–7]. Porous burners offer a practical technological route to address this issue [8–10]. Strong heat recirculation in porous burners allows premixed combustion of fuel mixtures that might not otherwise be flammable [5,11]. Currently, many industrial applications employ porous burners [12,13]. Examples include glass and chemical processing [14], gas turbines and propulsion [15,16] as well as heat exchangers [17]. In all these applications, combustion occurs under steady state conditions. However, switching from fossil fuels to biogas and biosyngas often includes utilisation of unsteady sources of fuels [18,19]. The unsteadiness could be in the fuel flow rate and/or chemical composition and is largely due to the temporal change in the feedstock that produce renewable fuels [19,20]. Unlike that under steady state, time-dependent combustion in porous media has, so far, received very little attention.

The general area of combustion in inert and catalytic porous media has already received substantial attention, see for example [21–25]. However, existing investigations have predominately focussed on steady combustion [26,25,27,28] where most studies have analysed burner operation with the use of methane mixtures [29–32] and very few incorporate ultra-lean operation [33]. As a result, there appears to be a gap in understanding the dynamic response of porous burners operating under time-varying and ultra-lean conditions. An air and fuel mixture is considered to be lean when $\phi < 1$. However, in ultra-lean combustion the fuel concentration is at or below the lean flammability limit for a free

* Corresponding author at: James Watt School of Engineering, University of Glasgow, Glasgow G12 8QQ, United Kingdom.
E-mail address: Nader.Karimi@glasgow.ac.uk (N. Karimi).

https://doi.org/10.1016/j.applthermaleng.2020.116099
Received 25 June 2020; Received in revised form 7 September 2020; Accepted 19 September 2020
Available online 28 September 2020

Nomenclature

List of symbols

a	amplitude
f	frequency (Hz)
$\dot{m}$	mass flow rate (kg s^{-1})
m	mass (kg)
P	thermal power (kW)
t	period (s)
T	temperature (K)
u	flow velocity (m s^{-1})
u_m	mixture velocity = air and fuel flow velocity (m s^{-1})
x,y	Cartesian coordinates

Greek symbols

ε	porosity
ϕ	equivalence ratio

Subscripts

F	fluid

Abbreviations

CO	carbon monoxide
CO_2	carbon dioxide
CH_4	methane
LHV	lower heating value
MFC	mass flow controller
ppi	pores per inch
ppm	parts per million
NO_x	nitrogen oxides

flame, i.e. for methane $\phi \leq 0.5$ [1]. Hence, it is imperative to understand unsteady combustion in porous burners. Here, a concise review of literature on the experimental studies related to premixed combustion in porous media over the past decade is put forward in a chronological order. Reviews of earlier works can be found in Refs. [34–37].

Bubnovich et al. [38] carried out an experiment with the aim of achieving flame stabilisation of premixed air and methane mixture within a porous burner between alumina balls of different sizes. A packed bed of alumina balls was utilised throughout the burner with a shorter diameter upstream (2.5 mm) and larger diameter downstream (5.6 mm). The burner was covered with insulation material to minimise heat losses and inserted thermocouples were utilised to measure the temperature inside the porous medium. CO and NO_x emissions were also measured at the exit of the burner using a gas analyser. Bubnovich et al. [38] found the flame to stabilise at the interface of the Alumina balls for the flow rates between 7.01 and 19.00 l/min where $0.6 < \phi < 0.7$. The authors [38] also found the pollutant emissions to be extremely low within this stability range where the maximum flame temperature was recorded to be 1675 K. Mujeebu et al. [39] investigated the combustion and emission characteristics of two novel porous burners with that of a conventional burner. The surface burner was made-up of two sheets of alumina foam; with the lower sheet consisting of a higher porosity and the upper sheet of a lower porosity. The authors [39] measured the temperature at four different locations by inserting thermocouples in the axial direction and the inlet fuel was a pre-vaporised liquid petroleum gas mixture. The flame stability, thermal efficiency, pollutant emissions and maximum flame temperature were compared with that of a conventional burner. A reduction of NO_x emissions of up to 75% for both porous burners compared with a conventional burner was reported.

A two-layer porous burner for low pollutant emissions was developed by Keramiotis et al. [40] who monitored its thermal efficiency and operational limits. A silicon carbide ceramic foam was used as the solid matrix with a density of 10ppi and methane and liquefied petroleum gas were chosen as the input fuels. The authors [40] varied different input parameters including equivalence ratio for lean combustion (0.625–0.83), excess air and thermal load output (200–1000 kW/m^2). The burner response was monitored by measuring the solid phase temperature and pollutant emissions. Keramiotis et al. [40] discovered excellent fuel interchangeability between liquefied petroleum gas and methane with respect to pollutant emissions and burner operation. It was concluded that for both fuels the burner is more sensitive to the changes in thermal load rather than equivalence ratio.

Robayo et al. [41] studied the enhancement of combustion in porous media by introducing perovskite catalysts to the ceramic matrix. A large porosity silicon carbide ceramic foam was utilised as the burner matrix with a steady lean methane/air mixture as the inlet fuel. Temperature was measured via thermocouples across eight axial points. Robayo et al. [41] found that all perovskite catalysts enhance the burner performance. Dehaj et al. [42] conducted an experimental study of premixed combustion of methane in a porous burner with the addition of a heat exchanger for household heating application. They [42] found the pressure to decrease within the burner as there is an increase in power and the excess air ratio.

A variable porosity porous burner was built by Song et al. [2] to operate on ultra-low calorific gas combustion. Silicon carbide was utilised as the ceramic foam whereby it gradually increases in pore density throughout, from the entrance to the exit of the burner. The purpose was to combust ultra-low calorific fuels lower than 6.28 MJ/m^3. In order to accommodate this, the authors [2] preheated the burner by igniting liquefied petroleum gas then switched to a $CH_4 + N_2$/air (ultra-low calorific) mixture, burning the ultra-low calorific fuel within the porous burner. Song et al. [2] discovered their annular porous burner increased the flame stability limit with a further reduction in CO emissions. The authors [2] managed to successfully combust a mixture with a calorific value as low as 1.4 MJ/m^3.

In an experimental study, Ghorashi et al. [43] compared pollutant emissions of a conventional and a custom built porous burner. These authors [43] monitored the effects of pore density and porous material on the pollutant emissions when the burner was fed by a steady flow of natural gas/air mixture. Silicon carbide and alumina were chosen as the solid porous matrix with pore density ranging between 10 and 30ppi and the burner operation was betweenϕ = 0.65–0.83. Ghorashi et al. [43] found the CO emissions to reduce by the use of alumina instead of silicon carbide. They also reported a surge in CO emissions with the increase in pore density. Chaelek et al. [44] developed a novel pre-heating air porous medium burner to compare its performance with a conventional burner. They designed an annular burner filled with alumina spheres whereby pre-heated air recirculates towards the inlet of the burner. The authors [44] measured the temperature at 14 different points via thermocouples to monitor the thermal performance of the burner and the exhaust gases were fed into a gas analyser. Chaelek et al. [44] found the maximum thermal efficiency of the burner to reach 51% whereby a reduction in energy consumption by 28.6% was noted when compared to a conventional burner.

In their experimental investigation, Devi et al. [45] ran a porous burner on a power range between 5 and 10 kW and a stable lean operating range of $0.75 < \phi < 0.97$ with biogas as fuel. These authors [45] analysed the performance of a conventional burner using the identical input parameters for comparative analysis. Devi et al. [45] discovered that their porous radiant burner reduced CO and NO_x emissions up to 95% and 85% respectively when compared to a conventional burner. Uniform temperature distribution on the surface of the burner was

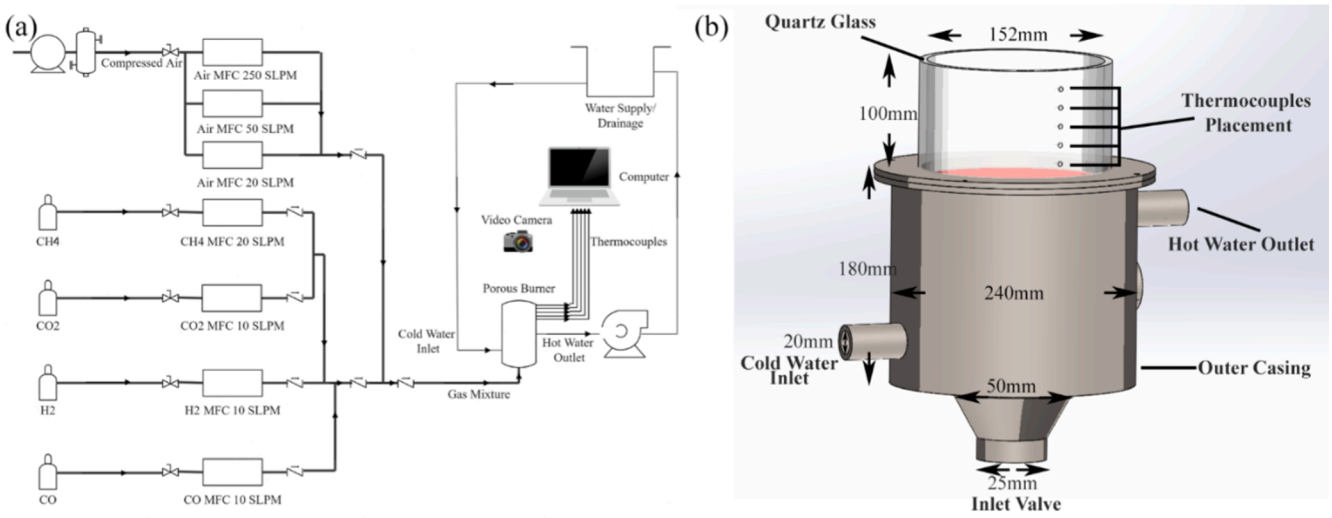

Fig. 1. (a) Schematic of the experimental setup (b) 3-D model of the porous burner.

considered as a sign of enhanced combustion performance. Hongsheng et al. [46] designed a porous burner operating on diesel fuel subject to pulse combustion. The core part of the burner consisted of alumina filled spheres filled within a quartz tube with a ceramic foam upstream to form the pre-heating zone. Hongsheng et al. [46] fed air and liquid diesel into the burner and once flame stability was achieved, the air flow was adjusted and the fuel was injected at intervals to create pulse combustion. It was shown that the propagation of the flame was similar to subsonic combustion under transient operation.

Most recently, Habib et al. [47–49] conducted extensive pore-scale modelling and demonstrated that the response of heat transfer in porous media to fluctuations in the inlet flow could involve complex dynamics. As combustion in porous media is dominated by heat transfer, it is anticipated that combustion is also significantly affected by fluctuations in the inlet flow. However, as clearly reflected by the preceding review of literature there is currently almost no systematic study of such effects. The present work aims to fill in this gap through an experimental approach.

2. Methodology

2.1. Experimental setup and instrumentation

Fig. 1 shows a schematic diagram of the employed experimental setup. The test rig and apparatus can be divided into four major parts; the fuel/air supply system, porous burner, water cooling supply and, data collection and measurement equipment.

2.1.1. Fuel/Air supply system

An air filter was used to extract moisture from compressed air. A quarter turn hand valve was installed upstream of air mass flow controllers (MFC) to manually operate the supply of air whereby an identical arrangement was made for fuel transmission between respective gas cylinders and MFCs with the installation of manual valves. ALICAT Scientific programmable MFCs were used for both fuel and air with an error margin of ±0.6%. Flow Vision SC software from ALICAT was utilised to alternate the mass flow rate (standard litres per minute – SLPM) of each MFC via a computer. Different ranges of MFCs (Fig. 1a) were operated to supply the steady and time-varying flows of air and fuel. Fuel was transported within a 6.35 mm diameter stainless steel pipe linking to a 25.4 mm outer diameter thick rubber pipe. The premixing of fuel and air took place within the rubber pipe before being fed into the porous burner.

2.1.2. Porous burner

The porous burner is comprised of four primary components including inlet valve, outer casing, combustion chamber and quartz glass. Fig. 1b displays a 3-D model of the burner and provides the key dimensions. All components were manufactured from stainless steel. A quartz glass was fixed on top of the burner with high temperature resistant sealant to visually observe the combustion process in porous media. The combustion chamber sits within the outer casing of the porous burner, leaving a gap for water to flow in-between for the cooling process. The water cooling process occurs around the exterior of the combustion chamber and interior of the outer casing of the porous burner. The empty void paves way for a water tank with attached inlet

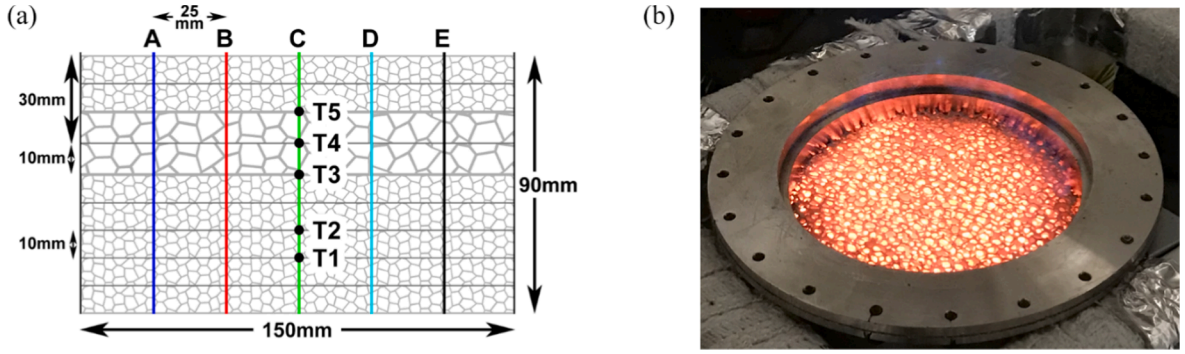

Fig. 2. (a) Schematic of the working section illustrating the position of thermocouples with reference points A, B, C, D, and E, (b) Top view of the porous burner during operation.

Table 1
Steady experiments.

			a-CH_4	b-Biogas (CH_4 = 70%,CO_2 = 30%)		
	CO_2 (standard L/min)	CH_4 (standard L/min)	Air (standard L/min)	Mixture (standard L/min)	Equivalence Ratio (ϕ)	Thermal Power (kW)
Case 1a		4.35	142.49	146.84	0.275	2.34
Case 2a		5.03	150.88	155.91	0.3	2.7
Case 3a		4.61	150.88	155.49	0.275	2.48
Case 4a		5.59	167.64	173.23	0.3	3
Case 5a		5.12	167.64	172.76	0.275	2.75
Case 6a		5.63	184.4	190.03	0.275	3.02
Case 7a		6.7	201.17	207.87	0.3	3.6
Case 8a		6.14	201.17	207.31	0.275	3.3
Case 9a		6.66	217.93	224.59	0.275	3.57
Case 10a		6.92	226.31	233.22	0.275	3.71
Case 1b	1.41	3.3	99.07	103.78	0.3	2.4
Case 2b	1.29	3.03	99.07	103.39	0.275	2.2
Case 3b	1.59	3.71	111.46	116.76	0.3	2.7
Case 4b	1.45	3.4	111.46	116.31	0.275	2.48
Case 5b	1.76	4.13	123.84	129.73	0.3	3
Case 6b	1.62	3.78	123.84	129.24	0.275	2.75
Case 7b	1.94	4.54	136.22	142.7	0.3	3.3
Case 8b	1.94	4.54	148.61	155.09	0.275	3.3
Case 9b	2.1	4.92	160.99	168.01	0.275	3.57

and outlet. Cold water flows from the water supply into the lower side of the burner via the inlet; filling up completely before exiting to ensuring maximum efficiency of the cooling process.

The combustion chamber was filled with layers of porous ceramic comprising of the preheating and combustion zones. Alumina foam (20ppi -$\varepsilon \approx 0.47$) sits at the bottom of the combustion chamber followed by a cone shaped silicon carbide ceramic foam (20ppi) to form the preheating zone and to mitigate the risks of flashback. This is preceded by a packed bed of less dense silicon carbide foams (10ppi $-\ \varepsilon \approx 0.72$). Further downstream, the quartz glass was filled with high density silicon carbide (20ppi) foams with the exception of two low density silicon carbide foams (10ppi) for flame stabilisation as shown in Fig. 2.

2.1.3. Data collection

Temperature measurements were carried out at five different points at the centre of the ceramic foam as shown in Fig. 2a. Type-N thermocouples were used with a 0.5 mm bead diameter because of their ability to withstand temperatures above 1553 K with an error margin of±2.5 K. The thermocouples were fed through the holes drilled in the quartz glass to the centre of the ceramic foam; fixed in place with high temperature resistant sealant. The voltage signals generated by each thermocouple were passed through an amplifier and plotted using Pico software. One hundred data points were recorded per second for each thermocouple to ensure high accuracy at a much higher frequency than that of the inlet fuel oscillations. An Anton Sprint Pro 5 multifunction flue gas analyser was positioned a few centimetres above the burner exit to measure CO, CO_2 and NO_x emissions for steady state cases. The gas analyser error margin was reported to be ±10ppm for CO range of 0–200 ppm, ±20 ppm for CO range of 200–2000 ppm, ±0.3% for CO_2 and ±5 ppm for NO_x. A high resolution (1920 × 1080) digital camera was used to record the flame behaviour and movement at a distance of approximately 1.5 m from the burner.

2.2. Experimental procedure

The fuel mixture equivalence ratio [50] was defined as

$$\phi = \frac{(m_f/m_{air})_{actual}}{(m_f/m_{air})_{stoichiometric}} \quad (1)$$

whereby the reactants form a lean mixture when the equivalence ratio is less than unity. The thermal load of the burner [50,51] is defined as

$$P = \dot{m}_f \times LHV_f \quad (2)$$

where $\dot{m}_f$, is the fuel mass flow rate and LHV_f, is the fuel lower heating value whereby the energy produced by the burner is calculated for each

Table 2
Oscillatory Experiments.

			x-CH_4	y-Biogas(CH_4 = 70%,CO_2 = 30%)				
	CO_2 (Standard L/m)	CH_4 (Standard L/m)	Air (Standard L/m)	Mixture (Standard L/m)	Equivalence Ratio (ϕ)	Thermal Power (kW)	Oscillation period (s) of CH_4 flow	Amplitude (%) of steady CH_4 flow
Case 1x		6.22–7.6	226.3	232.52–233.9	0.2475–0.3024	3.34–4.08	60 s	10%
Case 2x		4.84–8.98	226.3	231.14–235.28	0.1925–0.3572	2.6–4.82	60 s	30%
Case 3x		6.22–7.6	226.3	232.52–233.9	0.2475–0.3024	3.34–4.08	180 s	10%
Case 4x		4.84–8.98	226.3	231.14–235.28	0.1925–0.3572	2.6–4.82	180 s	30%
Case 1y	2.1	4.43–5.41	161	167.52–168.5	0.2475–0.3024	3.41–3.74	60 s	10%
Case 2y	2.1	3.44–6.4	161	166.53–169.49	0.1925–0.3572	3.07–4.06	60 s	30%
Case 3y	2.1	4.43–5.41	161	167.52–168.5	0.2475–0.3024	3.41–3.74	180 s	10%
Case 4y	2.1	3.44–6.4	161	166.53–169.49	0.1925–0.3572	3.07–4.06	180 s	30%

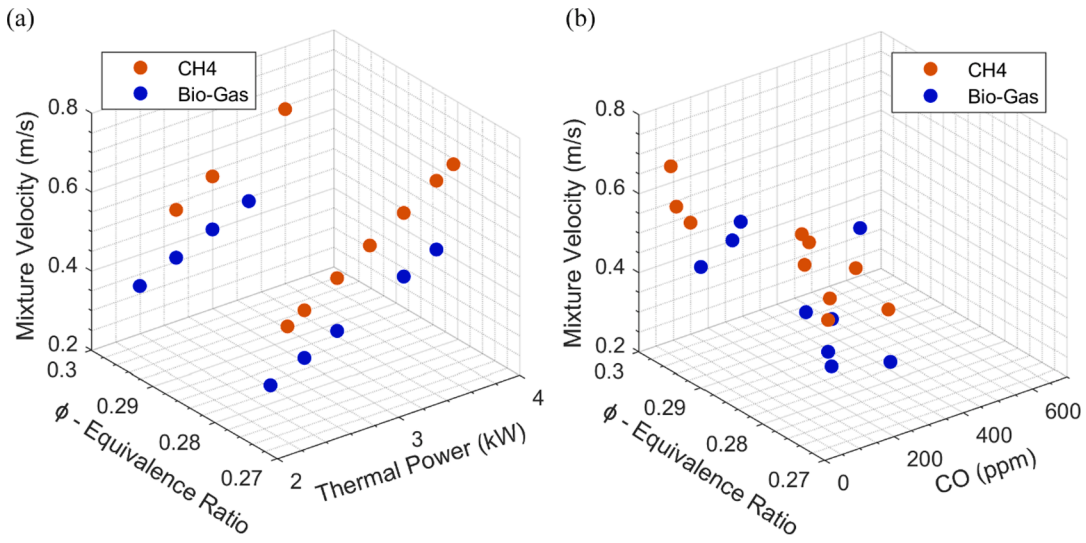

Fig. 3. Steady CH_4/Biogas mixtures (a) Equivalence Ratio vs Thermal Power (b) Equivalence Ratio vs CO emissions.

respective fuel.

Table 1 provides details of the experimental conditions for steady cases and Table 2 shows details for the unsteady cases, for both methane and biogas mixtures. Flow Vision SC software was used to program the MFCs to set the fuel flow rate systematically. The burner was ignited under lean conditions and the subsequent decrease in the fuel flow rate resulted in ultra-lean combustion and stabilisation of the flame inside the porous foam. The gas analyser measured pollutant emissions after the steady state cases had completely stabilised and the final temperature were recorded via the thermocouples.

As shown in Table 2, after achieving flame stability, the methane flow rate was oscillated between 10 and 30% of its base value at different frequencies for both mixtures. This was done by programming the digital mass flow controller to change the flow rate of methane according to a sinusoid with variable frequency and amplitude. The axial temperature profile was recorded for the entirety of the flame oscillation. The flame position movement was monitored along the reference points shown in Fig. 2 with a post-processing code developed in MATLAB.

2.3. Image processing

Extensive image processing was conducted to monitor the flame movement/position. Video footage was extracted for each unsteady case for a complete sinusoidal cycle – either 60 s or 180 s. A compilation of burner snapshots were created using Adobe Premiere Pro at a time interval of 2 s for each study to visualise the flame behaviour. Further, a code was developed in MATLAB to process the snapshots. After cropping each image to strictly the ceramic foam (see Fig. 2a), the image resolution was converted to represent distance whereby 5.34 pixels of each image corresponds to 1 mm in physical distance. In order to monitor the vertical flame movement, five equally spaced reference points were

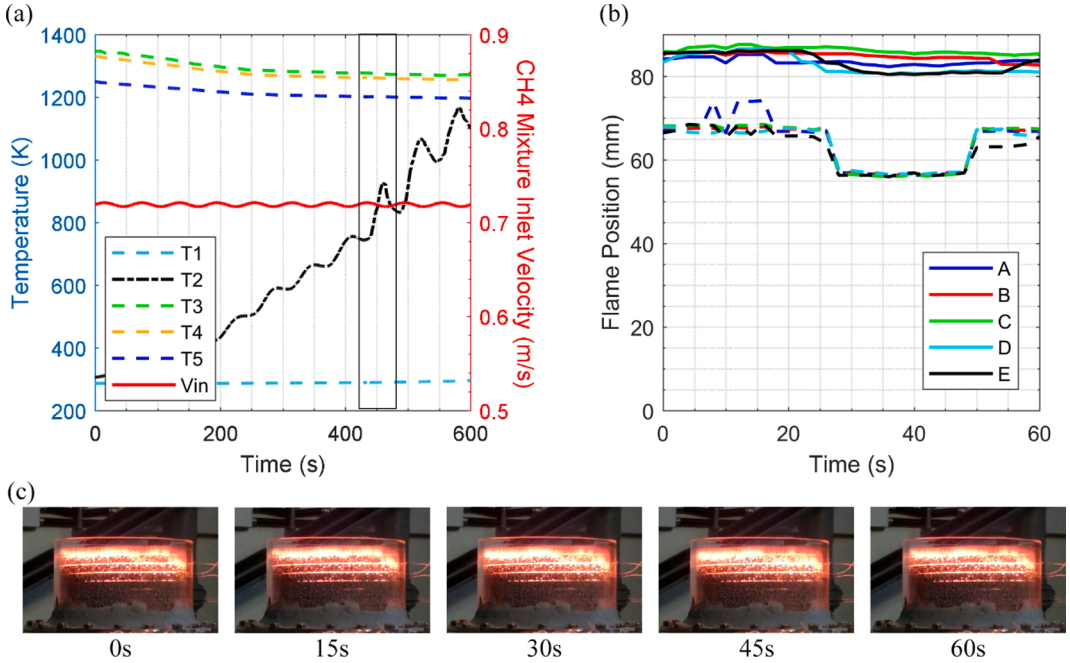

Fig. 4. Unsteady case 1x, a=10%, t = 60 s (a) Axial temperature profile vs CH_4 mixture velocity (b) Flame position movement at respective reference points, solid line – upper part of flame, dash line – lower part of flame (c) Snapshots of porous burner subject to unsteady flow at different intervals.

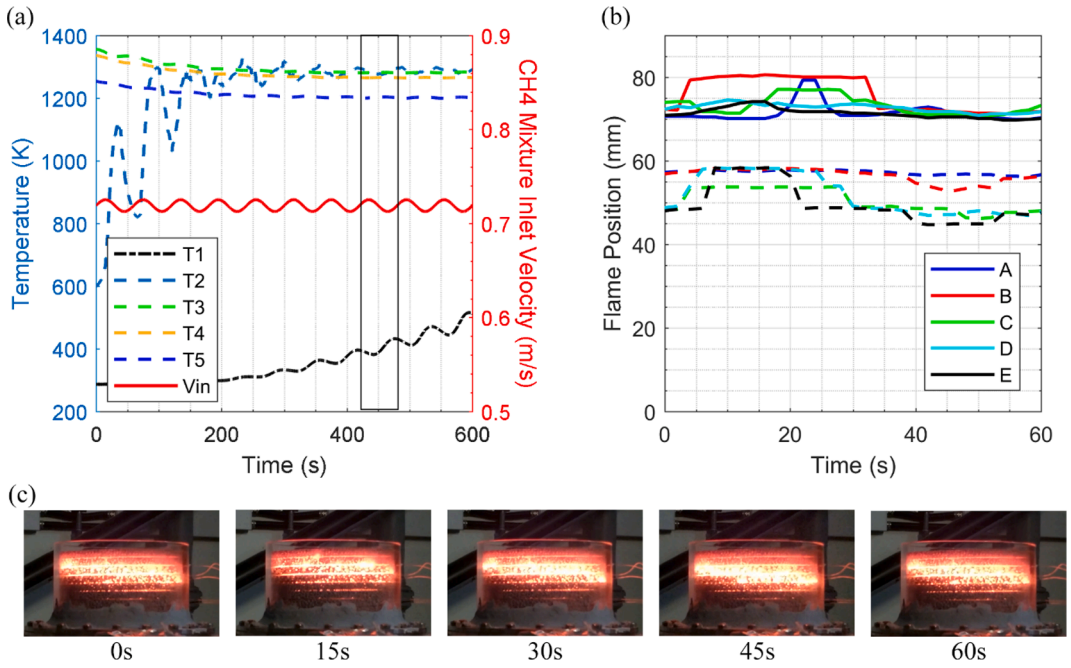

Fig. 5. Unsteady case 2x, a=30%, t = 60 s (a) Axial temperature profile vs CH_4 mixture velocity (b) Flame position movement at respective reference points, solid line – upper part of flame, dash line – lower part of flame (c) Snapshots of porous burner subject to unsteady flow at different intervals.

created along the x-axis in the y-direction. Each image was converted from colour to black and white, whereby a luminance criterion was set to detect the flame. The luminance value for flame detection differed for each fuel and was validated by visual confirmation. Once the luminance criterion was satisfied, the y-location of these values was calculated (where flame was detected) at the designated reference points. The values were further refined and only the upper and lower y-location was used to identify the top and bottom part of the flame at each reference point. The process was repeated for all snapshots for each case. The upper and lower locations of luminance values were then plotted in time, representing the flame movement in the y-direction of the ceramic foams across the five reference points over a complete sinusoidal cycle.

3. Results and discussion

The right quantity of heat generation, heat recirculation and heat losses are keys to achieving combustion stabilisation within porous media [1]. In general, combustion stabilisation can be achieved when the mixture velocity (air and fuel flow velocity) and flame speed are proportionate. Fig. 3 displays the burner performance under ultra-lean, steady state cases in which combustion stabilisation for both methane and biogas mixtures (Table 1) was achieved. Fig. 3a illustrates the relations between burner thermal power and mixture equivalence ratio and velocity. Here, the mixture (air and fuel) velocity refers to that inside the quartz tube. Expectedly, the thermal power increases monotonically as the mixture velocity is increased. It is also clear that methane mixtures feature relatively higher thermal power compared to those of biogas, which is simply due to the higher enthalpy of combustion of methane.

Fig. 3b highlights the effects of mixture velocity and equivalence ratio on CO emissions. The common trend shows the CO emissions plummet for a higher mixture velocity and for a lower equivalence ratio. As the mixture velocity reduces, the temperature within the combustion zone decreases. This is due to reduction in heat release while the heat losses remained almost unchanged. Lower temperatures contribute to incomplete combustion and interrupt oxidation of CO to CO_2. Lower equivalence ratio also reduces the heat generation and brings down the reaction temperature which then results in increase in CO emissions. Evidently, emission of CO is relatively high for biogas. This is because the existence of CO_2 in the mixture decreases the temperature compared to that in methane mixtures and increases the likelihood of incomplete combustion.

Case 10a (Table 1) was the starting point for all unsteady methane cases before introduction of the inlet sinusoidal disturbances. Fig. 4 illustrates the porous burner performance operating on methane mixture subject to inlet disturbance superimposed on the fuel flow rate with a period of 60 s and amplitude of 10%. The axial temperature was monitored throughout the entirety of the experiment whereby a flashback criterion was set at T1 = 773 K by empirical observation. Modulation of fuel flow rate resulted in a visible motion of the reactive front inside the quartz tube. This motion was filmed (see Section 2) and the subsequent temperature variation were further recorded. In total, ten cycles of oscillation in fuel flow rate were completed with the burner operation remaining stable.

Fig. 4a shows the temperature traces recorded by the thermocouples (see Fig. 2a) as well as the calculated fluctuations in the mixture flow velocity. Clearly, the temperature has been recorded by T3, between the interface of high density and low-density silicon carbide ceramic foam. The interface amid the two ceramic foams offers a supplementary means of stabilising the combustion flame whereby the upstream region behaves as a flashback arrestor. This is primarily due to the sudden decrease in pore size upstream of the interface. While throughout the experiment all measured temperatures exhibit almost stationary behaviours, T2 continues to rise as a direct response to the fluctuations in the inlet sinusoidal fuel. The independency of temperature traces upon the fluctuations in fuel flow implies that the flame motion has not been sensed by the thermocouples recording those traces. In the current case, this means that fluctuations in flame location is limited to the vicinity of thermocouple T2. To further investigate this, Fig. 4b visualises the flame position movement corresponding to the eighth sinusoidal cycle at its designated reference points. After a period of roughly 27 s, the lower part of the flame takes a significant dip (12 mm) which can be visually observed in Fig. 4c. This correlates to the temperature recoded by T2 as Fig. 4b shows that the movement of the flame is around 10 mm, which explains why other thermocouples did not sense the motion of the flame. A comparison between the flow velocity signal in Fig. 4a (the part inside

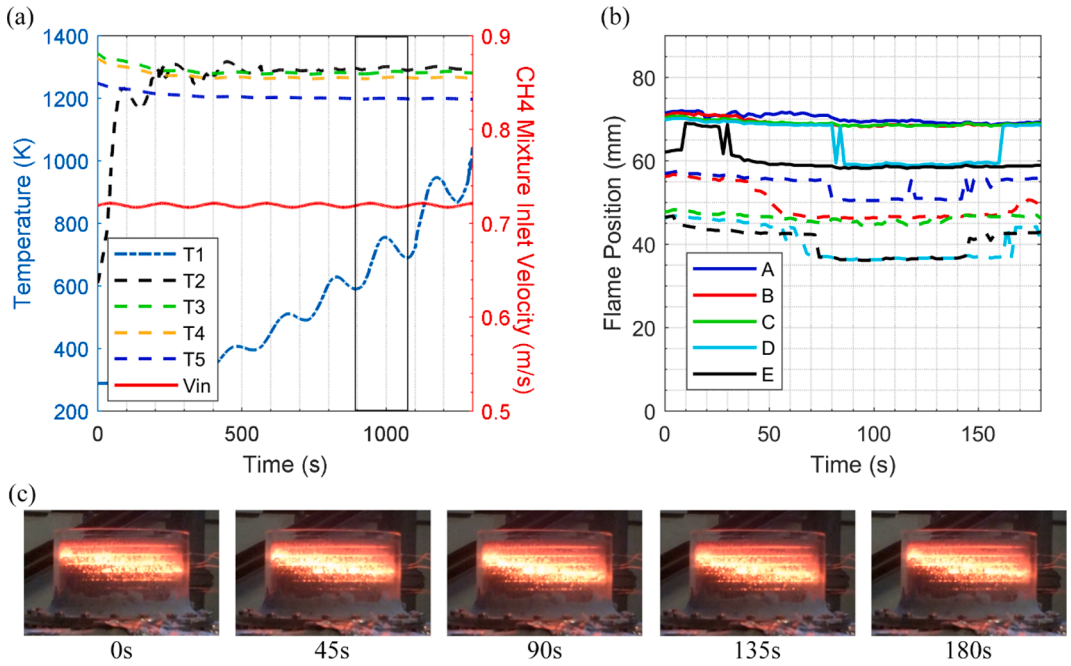

Fig. 6. Unsteady case 3x, a=10%, t = 180 s (a) Axial temperature profile vs CH_4 mixture velocity (b) Flame position movement at respective reference points, solid line – upper part of flame, dash line – lower part of flame (c) Snapshots of porous burner subject to unsteady flow at different intervals.

the box) and flame location in Fig. 4b, reveals that the flame motion more and less follows the fluctuation in the mixture velocity. Indeed, there is a phase lag between the two fluctuations. Yet, this is very much to be expected as time lag between the flow and flame oscillations are well recorded by studies on flame dynamics, e.g. [52].

Fig. 5 shows a similar case to case 1x albeit with a 30% inlet fuel flow rate illustrated in red. In Fig. 5a, the temperature is initially observed at T3, but as the time elapses, the temperature traces recorded by T2 and T3 as T2 become more responsive to the inlet disturbance. Heat recirculation is increased with the amplification of the inlet fuel flow rate. Downstream of the reaction zone, the combustion products are likely to have a higher temperature than the low density ceramic foam, thus convective heat transfer takes place between the hot gases and the solid matrix. The solid foam then radiates and conducts heat upstream of the combustion zone. Since the temperature of the solid is larger than that of the inlet mixture; convective heat transfer takes place between the solid and gas. As a result, the incoming cold reactants are preheated. However, due to the lower pore size and high density ceramic foam upstream, the rate of conductive heat transfer is increased as direct impact of large inlet fuel disturbance over a relatively short time. Consequently, the upstream thermocouple, T1 highlights the thermal response of the inlet disturbance over ten oscillatory cycles. Fig. 5c demonstrates the

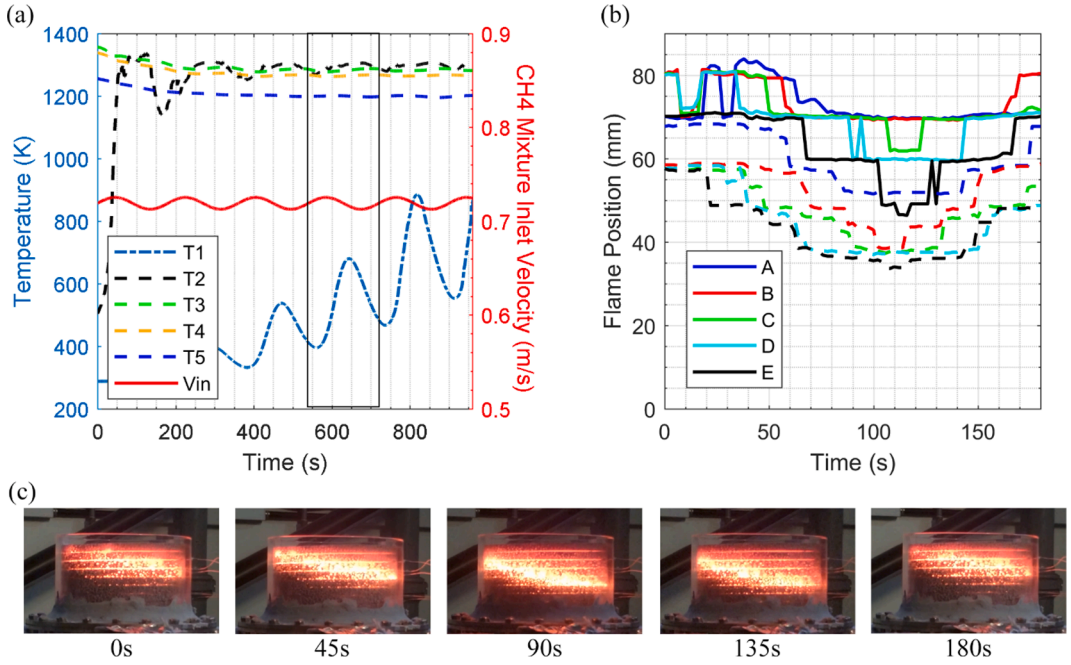

Fig. 7. Unsteady case 4x, a=30%, t = 180 s (a) Axial temperature profile vs CH_4 mixture velocity (b) Flame position movement at respective reference points, solid line – upper part of flame, dash line – lower part of flame (c) Snapshots of porous burner subject to unsteady flow at different intervals.

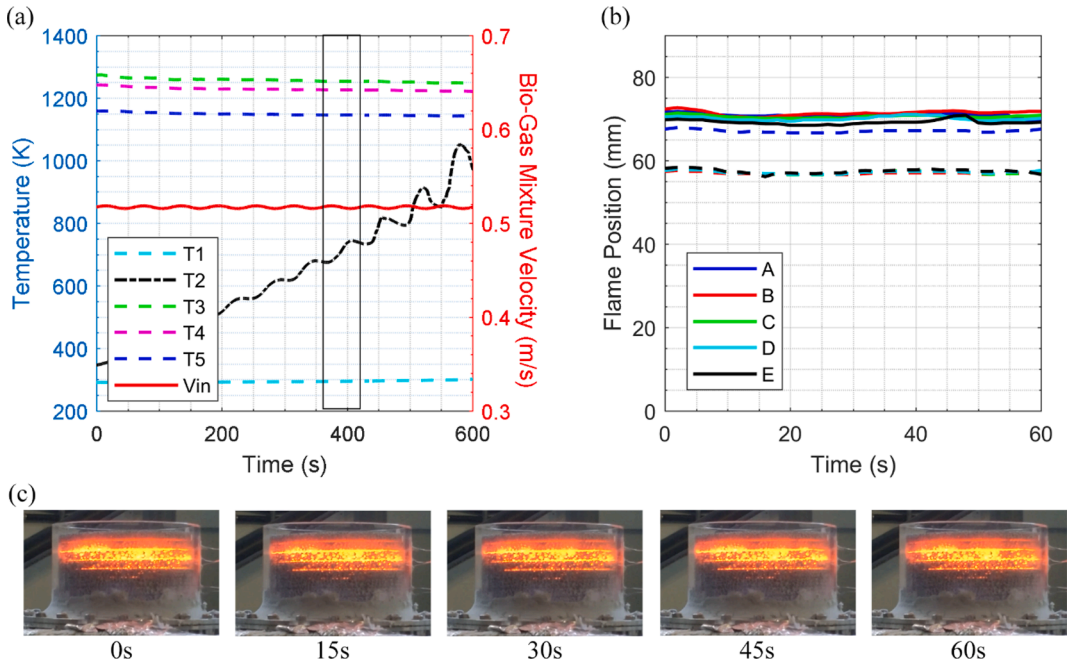

Fig. 8. Unsteady case 1y, a=10%, t = 60 s (a) Axial temperature profile vs Biogas mixture velocity (b) Flame position movement at respective reference points, solid line – upper part of flame, dash line – lower part of flame (c) Snapshots of porous burner subject to unsteady flow at different intervals.

flame movement of the eighth cycle of the inlet fuel fluctuations (marked by the box in Fig. 5a). A broken oscillatory pattern is visible as the flame position again directly correlates to the thermal response of the system. With the introduction of an increased amplitude the flame travels further upstream when compared to case 1x. As the core part of the flame has settled within the lower density silicon carbide, the flame thickness has also increased uniformly as can be seen in Fig. 5c.

Next, the period of fuel flow oscillation was extended to 180 s to provide a longer time for the combustion system to respond. Fig. 6a (case 1c) shows the temperature transitions from T3 to T2 post 500 s of the experiment. At this point, the combustion zone transitions into the upstream high density ceramic foam. Although the inlet disturbance is at a minimal amplitude of 10%, the prolonged fluctuation period extends the internal heat recirculation of the hot combustion products to the incoming cold reactants and minimises heat losses even when the inlet velocity is brought to low values. The oscillatory temperature response at T1 can be seen to increase rapidly as the combustion zone moves to the lower porosity silicon carbide foam, improving heat conduction and thermal radiation with the increase in foam density. Fig. 6b provides a visual of the sixth cycle of the inlet velocity impact upon the flame movement. Although, the flame position oscillates according to the imposed sinusoidal disturbance, a non-uniform movement is detected.

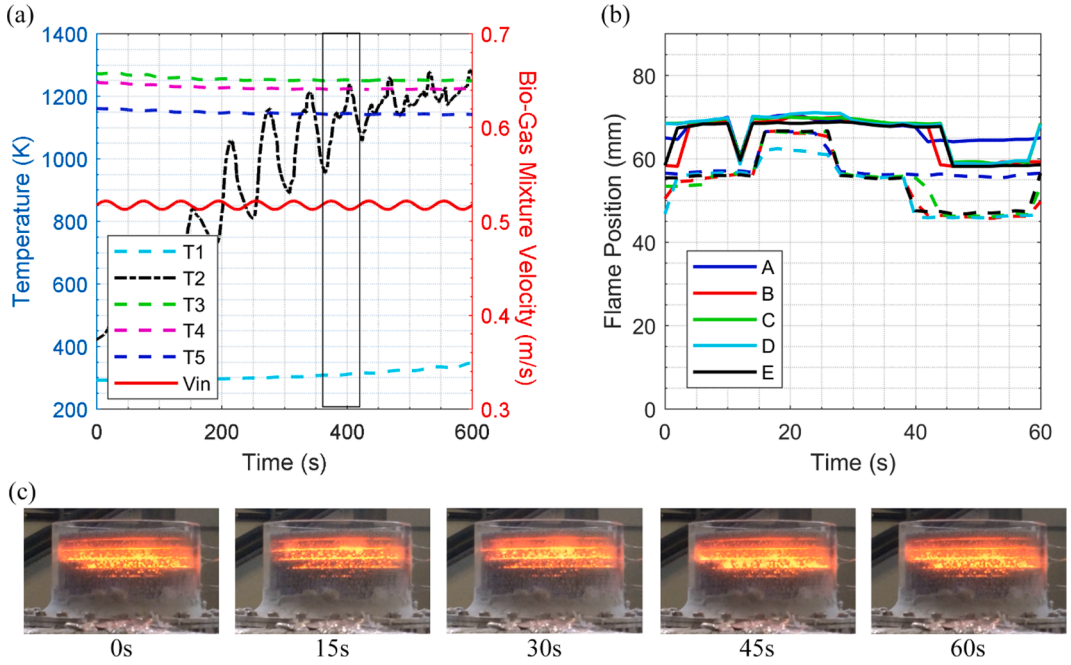

Fig. 9. Unsteady case 2y, a=30%, t = 60 s (a) Axial temperature profile vs Biogas mixture velocity (b) Flame position movement at respective reference points, solid line – upper part of flame, dash line – lower part of flame (c) Snapshots of porous burner subject to unsteady flow at different intervals.

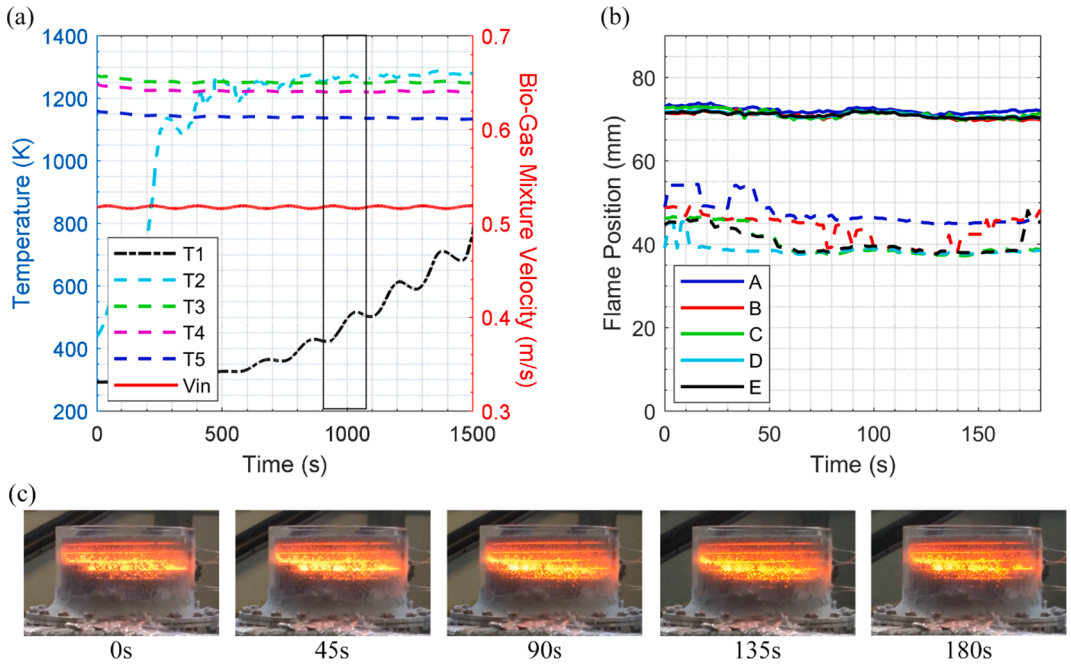

Fig. 10. Unsteady case 3y, a=10%, t = 180 s (a) Axial temperature profile vs Biogas mixture velocity (b) Flame position movement at respective reference points, solid line – upper part of flame, dash line – lower part of flame (c) Snapshots of porous burner subject to unsteady flow at different intervals.

This is further verified by Fig. 6c whereby the flame features a roughly 30 degree tilt. This behaviour could be due to the existence of small imperfections in the ceramic foam orientation with the insertion of thermocouples allowing the preheating of incoming cold reactants to accelerate on one side of the burner foam. Nonetheless, such tilting was not observed in steady state cases and its inception is related to long-period forcing.

Fig. 7 highlights (case 4x) the thermal response and flame oscillations as a result of a modulation of fuel flow with the amplitude of 30% over a cycle period of 180 s. With the increase of amplitude in the methane fuel rate, the equivalence ratio surges to 0.3572 at the peak of the sinusoidal wave, far higher than the stable operating range for the burner for a methane mixture. At the trough of each sinusoidal wave, the equivalence ratio drops to 0.1925, quenching the local flame. Yet, with an increased period of fluctuations, in each cycle the porous burner stores the heat and with the increase of the fuel flow rate; accelerates the excess enthalpy combustion. As a result, in Fig. 7a, after five cycles the fuel flow is cut off as the burner reaches the flashback criterion within 900 s, far quicker than when the amplitude was set at 10% (1300 s). Fig. 7b portrays the fourth sinusoidal cycle of the flame movement. It can be seen that the non-uniform movements of the flame augments amongst the reference points with an increase in amplitude. Fig. 7c displays this behaviour where the flame not only causes a further tilt but also visualises the further spread of the flame amongst the porous burner within the ceramic foam.

Case 9b (see Table 1) is used as the foundation for all unsteady biogas mixture cases before the inlet sinusoidal disturbances are introduced. Fig. 8 represents biogas mixture subject to sinusoidal disturbance of 10% amplitude of methane flow over a period of 60 s (case 1y). The carbon dioxide composition of the mixture and air are kept constant amongst all biogas experiments. Upon initial observation, Fig. 8a shows the inlet fuel oscillations have little or no effect across all thermocouples except T2. For this case, the flame was subject to 10 forcing cycles while maintaining stable operation. A comparison between biogas and methane mixture displays a similar pattern with the rate of increase in temperature at T2, however from the eighth cycle onwards, a noticeably lesser temperature increase is observed in biogas mixture. This can be primarily attributed to the chemical composition of the mixture; as a smaller amount of fuel is being burned of the incoming reactants, less heat is generated. This led to smaller temperature rises and a longer time for heat to transfer. As a domino effect, this also increases the time to heat up the silicon carbide foam. Fig. 8b displays that the flame movement is minimal within the seventh cycle as the reaction rate of biogas mixture is slower. A 10% amplitude has minimal impact, albeit due to the extensive thermal properties of silicon carbide it manages to withhold heat. Fig. 7c depicts the biogas flame showing no obvious flame movement over the relevant period. However, it is noted that the flame colour and luminance is less intense when compared with the methane mixture due to the dilution of the mixture.

Fig. 9 displays (case 2y) the trend of biogas flame as the amplitude of fluctuations in fuel flow is increased to 30% of its base value over a period of 60 s. Fig. 9a highlights stable burner operation throughout the experiment, completing ten cycles of the superimposed disturbances on fuel flow. The flame realigns itself with T2 being the most responsive thermocouple to the inlet disturbance whereby a sporadic oscillatory pattern is observed post cycle six of the experiment. During this period, a gradual increase in temperature at T1 is observed. It should be noted that due to the increase of amplitude of the fuel flow rate a greater increase and decrease in temperature is detected whereby a larger temperature amplitude is visible in T2 when compared to case 1y. Further, as a result of the short period of fluctuations, the silicon carbide foam is able to retain heat. Extending the gradual reduction in reaction rate, the burner overcomes flame extinction as the fuel flow rate rebounds into a surplus value from the foundation model (case 9b). This borderline uncertainty is also visible in Fig. 9b and c where the flame thickness is minimal for the seventh cycle of the experiment as the burner responds to the reduction in the flow rate from the previous cycle. After recovery, the temperature increases, the flame thickness widens and the flame position moves upstream.

Fig. 10 shows (case 3y) the effect of increasing the time period of the inlet fuel flow rate disturbance to 180 s with a 10% amplitude. Overall the system (Fig. 10a) is able to complete 8 cycles of oscillatory flow amidst experiencing gradual flashback and the flame travelling upstream. Biogas mixture was able to prevent flashback for an additional 6 min when compared to methane mixture for similar conditions. This is primarily due to a variety of factors such as lower inlet velocity, lower

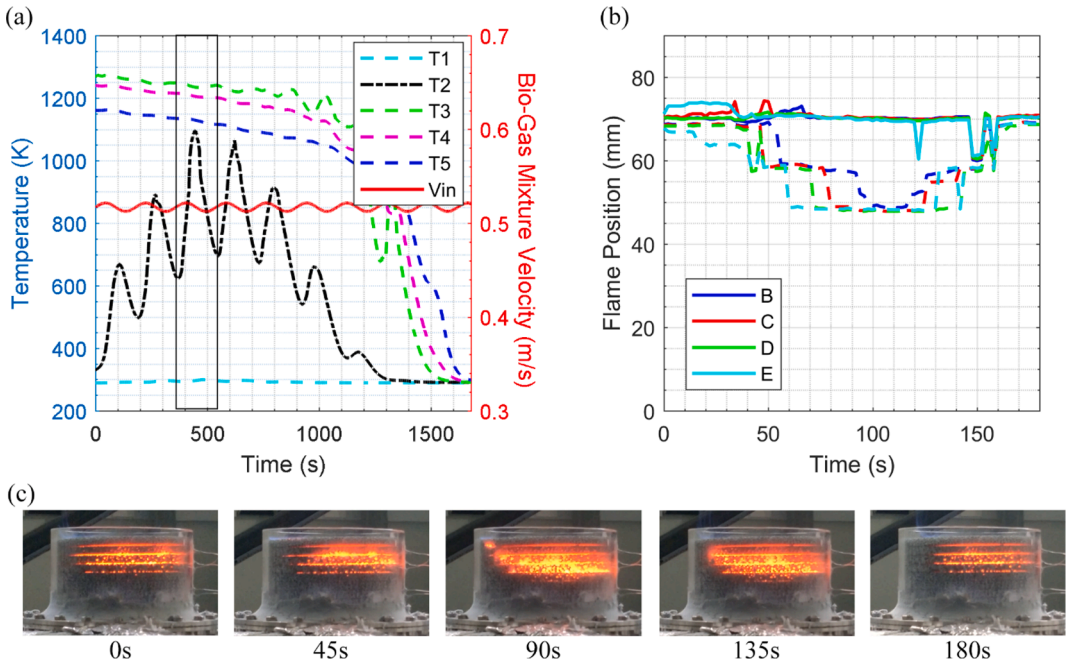

Fig. 11. Unsteady case 4y, a=30%, t = 180 s (a) Axial temperature profile vs Biogas mixture velocity (b) Flame position movement at respective reference points, solid line – upper part of flame, dash line – lower part of flame (c) Snapshots of porous burner subject to unsteady flow at different intervals.

flame speed and dilution of fuel composition; all lowering the flame temperature and speed. As a result, heat transfer within the ceramic foam also occurs at a slower pace due to the weaker temperature gradient between the flame and foam. Further, prolonging the flashback effects with the ceramic foam taking longer to achieve thermal equilibrium with the flame moving upstream. T1 directly responds to the induced disturbance almost taking the shape of an asymptotic curve if allowed to continue. The flame position of the sixth cycle of the experiment is shown in Fig. 10b. The flame movement appears to be minimal due to the low amplitude fluctuation albeit there is a significant increase in flame thickness, indicating a slower reaction rate. This is further confirmed by visual inspection by Fig. 10c at various time intervals whilst the burner is subject to modulation of the fuel flow.

Fig. 11 represents case 4y whereby the amplitude is increased to 30% of the inlet fuel flow rate at a period of 180 s per cycle. Fig. 11a shows the burner response commences with T2 recording temperature gains of the first three cycles and then the system begins to experience more heat loss than heat addition. As a result, complete flame extinction via blow off occurs at the seventh cycle. As the fuel flow rate was adjusted for the methane mixture only, the equivalence ratio was altered but for biogas both the equivalence ratio and ratio of methane to carbon dioxide were affected. At the trough of the highest amplitude (30%) of fuel modulation, the equivalence ratio drops to 0.1925. With such a low ratio of fuel compared to the rest of the mixture over a longer time, the burner is not able to recover the lost heat when the inlet inputs a surplus flow of methane into the system. Furthermore, with each cycle the overall temperature continues to drop, with the combustion gas transferring little or less heat to the pre-heating zone. This process continues to repeat until the overall temperature drop is so significant that it can no longer ignite the incoming mixture within the conduits of the ceramic foam; resulting in flame extinction. Fig. 11b further clarifies this as no flame is detected at reference point A during the third cycle, where a gradual blow off is underway. Although, due to the higher amplitude a larger flame thickness is detected albeit very minimal flame movement [53]. A drastic heat loss during the imposed sinusoidal disturbance is visible at various time intervals as can be seen in Fig. 11c.

4. Conclusions

An experimental study was conducted on a porous burner under ultra-lean condition to investigate the effects of sinusoidal fluctuations in the inlet fuel flow upon the flame dynamics. Such burners can be used in heating applications where very high temperatures are not needed. Burner operation with biogas often involves unsteadiness in fuel flow rate because of the inherent fluctuations in the gas supply of small-scale anaerobic digesters. Methane and a mixture of methane and carbon dioxide, mimicking biogas, were used as fuel. The fluctuations were superimposed on the fuel flow via programmable mass flow controllers. The response of the porous burner was evaluated by measuring the temperature at different axial locations along the burner centreline and by capturing the flame movement through imaging. It was shown that, under steady conditions, the burner could be operated for equivalence ratios as low as 0.275 for both methane and biogas. Further, biogas ultra-lean flames generated more CO emissions than methane flames. Under unsteady conditions, the porous burner was able to stabilise combustion when the methane mixture was subjected to inlet sinusoidal disturbances with amplitudes between 0 and 30% of the steady values over a period of 60 s. It was found that the vertical motion of the flame roughly follows the dynamics of the imposed oscillations. This was the case for both methane and the biogas mixture. However, the extent of flame movement for methane was significantly greater than that for biogas, whereas the flame thickness increase/decrease for biogas was more responsive than for methane. Finally, for both fuels, long exposure of the burner (180 s) to fuel flow modulations led to flame destabilisation, resulting in flashback or blow-off.

Declaration of Competing Interest

The authors declare that they have no known competing financial interests or personal relationships that could have appeared to influence the work reported in this paper.

Acknowledgment

N. Karimi and B. Yadollahi acknowledge the financial support of

Engineering and Physical Science Research Council through grant EP/N020472/1.

References

[1] S. Wood, A.T. Harris, Porous burners for lean-burn applications, Prog. Energy Combust. Sci. 34 (5) (2008) 667–684.
[2] F. Song, Z. Wen, Z. Dong, E. Wang, X. Liu, Ultra-low calorific gas combustion in a gradually-varied porous burner with annular heat recirculation, Energy 119 (2017) 497–503.
[3] R. Rosa, The role of synthetic fuels for a carbon neutral economy, C 3 (4) (2017) 11.
[4] L. Wang, N. Karimi, M.C. Paul, Gas-phase transport and entropy generation during transient combustion of single biomass particle in varying oxygen and nitrogen atmospheres, Int. J. Hydrogen Energy 43 (17) (2018) 8506–8523.
[5] J.R. Howell, M.J. Hall, J.L. Ellzey, Combustion of hydrocarbon fuels within porous inert media, Prog. Energy Combust. Sci. 22 (2) (1996) 121–145.
[6] L. Christodoulou, L. Kabiraj, A. Saurabh, N. Karimi, Characterizing the signature of flame flashback precursor through recurrence analysis, Chaos An Interdiscip. J. Nonlinear Sci. 26 (1) (2016) 013110.
[7] N. Karimi, S. McGrath, P. Brown, J. Weinkauff, A. Dreizler, Generation of adverse pressure gradient in the circumferential flashback of a premixed flame, Flow Turbul. Combust. 97 (2) (2016) 663–687.
[8] S. Rashidi, F. Hormozi, M.H. Doranehgard, Abilities of porous materials for energy saving in advanced thermal systems, J. Therm. Anal. Calorim. (2020).
[9] S. Rashidi, M.H. Kashefi, K.C. Kim, O. Samimi-Abianeh, Potentials of porous materials for energy management in heat exchangers – a comprehensive review, Appl. Energy 243 (2019) 206–232.
[10] M. Siavashi, K. Karimi, Q. Xiong, M.H. Doranehgard, Numerical analysis of mixed convection of two-phase non-Newtonian nanofluid flow inside a partially porous square enclosure with a rotating cylinder, J. Therm. Anal. Calorim. 137 (1) (2019) 267–287.
[11] P. Gholamalipour, M. Siavashi, M.H. Doranehgard, Eccentricity effects of heat source inside a porous annulus on the natural convection heat transfer and entropy generation of Cu-water nanofluid, Int. Commun. Heat Mass Transf. 109 (2019) 104367.
[12] O. Mahian, L. Kolsi, M. Amani, P. Estellé, G. Ahmadi, C. Kleinstreuer, J.S. Marshall, M. Siavashi, R.A. Taylor, H. Niazmand, S. Wongwises, T. Hayat, A. Kolanjiyil, A. Kasaeian, I. Pop, Recent advances in modeling and simulation of nanofluid flows-Part I: Fundamentals and theory, Phys. Rep. 790 (2019) 1–48.
[13] A. Izadi, M. Siavashi, H. Rasam, Q. Xiong, MHD enhanced nanofluid mediated heat transfer in porous metal for CPU cooling, Appl. Therm. Eng. 168 (2020) 114843.
[14] S. Mößbauer, O. Pickenäcker, K. Pickenäcker, Application of the porous burner technology in energy- and heat engineering, in: 5th International Conference on Technologies and Combustion for a Clean Environment (Clean Air V), 1999, pp. 519–523.
[15] J. Ellzey, M. William, Porous Burner For Gas Turbine Applications, 2003024655, 2003.
[16] M.A. Mujeebu, M.Z. Abdullah, M.Z.A. Bakar, A.A. Mohamad, R.M.N. Muhad, M. K. Abdullah, Combustion in porous media and its applications – a comprehensive survey, J. Environ. Manage. 90 (8) (2009) 2287–2312.
[17] N. Delalic, D. Mulahasanovic, E.N. Ganic, Porous media compact heat exchanger unit – experiment and analysis, Exp. Therm. Fluid Sci. 28 (2–3) (2004) 185–192.
[18] C. Mao, Y. Feng, X. Wang, G. Ren, Review on research achievements of biogas from anaerobic digestion, Renew. Sustain. Energy Rev. 45 (2015) 540–555.
[19] K. Göransson, U. Söderlind, J. He, W. Zhang, Review of syngas production via biomass DFBGs, Renew. Sustain. Energy Rev. 15 (1) (2011) 482–492.
[20] L. Wang, N. Karimi, T. Sutardi, M.C. Paul, Combustion characteristics and pollutant emissions in transient oxy-combustion of a single biomass particle: a numerical study, Energy Fuels 33 (2) (2019) 1556–1569.
[21] M. Toledo, F. Gracia, S. Caro, J. Gómez, V. Jovicic, Hydrocarbons conversion to syngas in inert porous media combustion, Int. J. Hydrogen Energy 41 (14) (2016) 5857–5864.
[22] J. Dunnmon, S. Sobhani, M. Wu, R. Fahrig, M. Ihme, An investigation of internal flame structure in porous media combustion via X-ray Computed Tomography, Proc. Combust. Inst. 36 (3) (2017) 4399–4408.
[23] G. Hunt, N. Karimi, B. Yadollahi, M. Torabi, The effects of exothermic catalytic reactions upon combined transport of heat and mass in porous microreactors, Int. J. Heat Mass Transf. 134 (2019) 1227–1249.
[24] S. Bani, J. Pan, A. Tang, Q. Lu, Y. Zhang, Micro combustion in a porous media for thermophotovoltaic power generation, Appl. Therm. Eng. 129 (2018) 596–605.
[25] H. Liu, D. Wu, M. Xie, H. Liu, Z. Xu, Experimental and numerical study on the lean premixed filtration combustion of propane/air in porous medium, Appl. Therm. Eng. 150 (January) (2019) 445–455.
[26] P. Gentillon, J. Southcott, Q.N. Chan, R.A. Taylor, Stable flame limits for optimal radiant performance of porous media reactors for thermophotovoltaic applications using packed beds of alumina, Appl. Energy 229 (July) (2018) 736–744.
[27] Q. Peng, W. Yang, E. Jiaqiang, H. Xu, Z. Li, W. Yu, Y. Tu, Y. Wu, Experimental investigation on premixed hydrogen/air combustion in varied size combustors inserted with porous medium for thermophotovoltaic system applications, Energy Convers. Manag. 200 (June) (2019).
[28] J. He, Z. Chen, X. Jiang, C. Leng, Combustion characteristics of blast furnace gas in porous media burner, Appl. Therm. Eng. 160 (November) (2019).
[29] H. Wang, C. Wei, P. Zhao, T. Ye, Experimental study on temperature variation in a porous inert media burner for premixed methane air combustion, Energy 72 (2014) 195–200.
[30] Y. Liu, D. Ning, A. Fan, H. Yao, Experimental and numerical investigations on flame stability of methane/air mixtures in mesoscale combustors filled with fibrous porous media, Energy Convers. Manag. 123 (2016) 402–409.
[31] A.C. Terracciano, S. De Oliveira, D. Vazquez-Molina, F.J. Uribe-Romo, S.S. Vasu, N. Orlovskaya, Effect of catalytically active Ce0.8Gd0.2O1.9 coating on the heterogeneous combustion of methane within MgO stabilized ZrO2 porous ceramics, Combust. Flame 180 (2017) 32–39.
[32] A. Saeed, N. Karimi, G. Hunt, M. Torabi, On the influences of surface heat release and thermal radiation upon transport in catalytic porous microreactors—a novel porous-solid interface model, Chem. Eng. Process. – Process Intensif. 143 (2019) 107602.
[33] K. Xu, M. Liu, P. Zhao, Stability of lean combustion in mini-scale porous media combustor with heat recuperation, Chem. Eng. Process. Process Intensif. 50 (7) (2011) 608–613.
[34] M.A. Mujeebu, M.Z. Abdullah, M.Z.A. Bakar, A.A. Mohamad, M.K. Abdullah, Applications of porous media combustion technology – a review, Appl. Energy 86 (9) (2009) 1365–1375.
[35] M.A. Mujeebu, M.Z. Abdullah, M.Z.A. Bakar, A.A. Mohamad, M.K. Abdullah, A review of investigations on liquid fuel combustion in porous inert media, Prog. Energy Combust. Sci. 35 (2) (2009) 216–230.
[36] M.M. Kamal, A.A. Mohamad, Combustion in porous media, Proc. Inst. Mech. Eng. Part A J. Power Energy 220 (5) (2006) 487–508.
[37] D. Ingham, A. Bejan, E. Mamut, I. Pop, Emerging Technologies and Techniques in Porous Media, 2012.
[38] V. Bubnovich, M. Toledo, L. Henríquez, C. Rosas, J. Romero, Flame stabilization between two beds of alumina balls in a porous burner, Appl. Therm. Eng. 30 (2010) 92–95.
[39] M.A. Mujeebu, M.Z. Abdullah, A.A. Mohamad, Development of energy efficient porous medium burners on surface and submerged combustion modes, Energy 36 (8) (2011) 5132–5139.
[40] C. Keramiotis, B. Stelzner, D. Trimis, M. Founti, Porous burners for low emission combustion: an experimental investigation, Energy 45 (1) (2012) 213–219.
[41] M.D. Robayo, B. Beaman, B. Hughes, B. Delose, N. Orlovskaya, R.H. Chen, Perovskite catalysts enhanced combustion on porous media, Energy 76 (2014) 477–486.
[42] M. Shafiey Dehaj, R. Ebrahimi, M. Shams, M. Farzaneh, Experimental analysis of natural gas combustion in a porous burner, Exp. Therm Fluid Sci. 84 (2017) 134–143.
[43] S.A. Ghorashi, S.A. Hashemi, S.M. Hashemi, M. Mollamahdi, Experimental study on pollutant emissions in the novel combined porous-free flame burner, Energy 162 (2018) 517–525.
[44] A. Chaelek, U.M. Grare, S. Jugjai, Self-aspirating/air-preheating porous medium gas burner, Appl. Therm. Eng. 153 (November 2018) (2019) 181–189.
[45] S. Devi, N. Sahoo, P. Muthukumar, Combustion of biogas in Porous Radiant Burner: low emission combustion, Energy Procedia 158 (2019) 1116–1121.
[46] S. Devi, N. Sahoo, P. Muthukumar, Experimental studies on biogas combustion in a novel double layer inert Porous Radiant Burner, Renew. Energy 149 (2020) 1040–1052.
[47] R. Habib, N. Karimi, B. Yadollahi, M. Hossein, L.K.B. Li, A pore-scale assessment of the dynamic response of forced convection in porous media to inlet flow modulations, Int. J. Heat Mass Transf. 153 (2020) 119657.
[48] R. Habib, B. Yadollahi, N. Karimi, M. Hossein, On the unsteady forced convection in porous media subject to inlet flow disturbances-A pore-scale analysis, Int. Commun. Heat Mass Transf. 116 (2020) 104639.
[49] R. Habib, B. Yadollahi, N. Karimi, A pore-scale investigation of the transient response of forced convection in porous media to inlet ramp inputs, J. Energy Resour. Technol. (2020) 1–14.
[50] M.J. Moran, H.N. Shapiro, D.D. Boettner, M.B. Bailey, Fundamentals of Engineering Thermodynamics, 7th ed., 2011.
[51] S.R. Turns, An Introduction to Combustion: Concepts and Applications, 2nd ed., McGraw Hill, 2000.
[52] N. Karimi, Response of a conical, laminar premixed flame to low amplitude acoustic forcing – a comparison between experiment and kinematic theories, Energy 78 (2014) 490–500.
[53] Y. Kazemian, S. Rashidi, J.A. Esfahani, O. Samimi-Abianeh, Effects of grains shapes of porous media on combustion onset—a numerical simulation using Lattice Boltzmann method, Comput. Math. with Appl. (2019).